

Investigation of equation of state and in-medium NN cross sections through nuclear stopping

M. H. Zhao (赵明辉),^{1,2,*} F. Fu (付芬),¹ M. Huang (黄美容),^{1,†} R. Wada,¹ W. Lin (林炜平),^{1,2} X. Liu (刘星泉),^{1,2} J. S. Wang (王建松),¹ Y. Li (李勇),^{1,2} Y. Y. Yang (杨彦云),¹ S. L. Jin (金仕纶),¹ J. B. Ma (马军兵),¹ P. Ma (马朋),¹ Q. Wang (王琦),¹ and Z. Chen (陈志强)¹

¹*Institute of Modern Physics, Chinese Academy of Science, Lanzhou 730000, People's Republic of China*

²*University of Chinese Academy of Science, Beijing, 100049, People's Republic of China*

(Received 28 January 2014; published 28 March 2014)

By using an antisymmetrized molecular dynamics model (AMD), the data of kinematically complete events are compared with the experimental INDRA data through nuclear stopping in Xe + Sn collisions at 10 to 100A MeV. The sensitivity of the nuclear stopping is studied through interactions with different equations of state (EOSs) (soft and stiff) and in-medium NN cross sections in different energy domains. Above 25A MeV, both EOSs and different NN cross sections can affect the nuclear stopping, but none of these parameters used in the AMD model can reproduce the experimental data at 20 to 30A MeV. On the other hand, below 25A MeV, nuclear stopping is not sensitive to both of the EOSs and the NN cross sections because of complete nuclear stopping. This indicates that some important mechanisms may be missing in AMD or that the selection of central collision events may be significantly different between the experiments and the simulations at this energy range.

DOI: [10.1103/PhysRevC.89.037001](https://doi.org/10.1103/PhysRevC.89.037001)

PACS number(s): 25.70.-z, 21.65.Mn, 21.30.-x

Introduction. To understand the properties of nuclear matter, the study of the transport mechanism of nucleons in nuclear reactions is very important. Transport properties are vital to illustrate the mechanism of supernova collapse and the formation of a neutron star [1–3]. As one of the observables, such as multiplicity distributions and collective flows, in heavy-ion collisions (HICs) at intermediate energies [4], nuclear stopping governs the quantity of dissipation energy and the amplitude of collective motions and controls the reaction mechanisms, such as deep inelastic reactions, neck formation, and fusion reactions [2]. Nuclear stopping can also provide information on the equation of state (EOS) of nuclear matter, the in-medium NN cross section, and the level of equilibration reached in nuclear reactions [2,5–8].

By comparing the predictions of microscopic transport models, such as the antisymmetrized molecular dynamics model (AMD) [9,10], with experimental data of HICs at intermediate energies, one can improve the knowledge of basic ingredients of such models, such as EOSs and the in-medium NN cross section. For example, a broad systematic study in system size and incident energy for nuclear stopping has been performed by the INDRA and ALADIN Collaborations [2], which can be used to determine these parameters in the AMD model [11].

In this paper, we analyze nuclear stopping in the Xe + Sn system at 10 to 100A MeV using the INDRA data and make comprehensive comparisons with AMD simulations. Since the stiffness of the EOS and the in-medium NN cross section are both important ingredients for the degree of nuclear stopping power in the calculations [11], we mainly explore their sensitivity to nuclear stopping.

Analysis method. To quantify the nuclear-stopping power, the energy-based isotropy ratio R_E , which is the ratio of the

transverse energy to the parallel energy, is defined as

$$R_E = \frac{\sum E_{\perp}}{2 \sum E_{\parallel}}, \quad (1)$$

where E_{\perp} (E_{\parallel}) is the transverse (parallel) energy in the center-of-mass (c.m.) system and the sum runs over all products under the condition described below. Equation (1) is used in the INDRA experiment [2] to measure nuclear stopping; so it does in our AMD analysis. The AMD model has many applications in nuclear physics research [9–17]. In this paper, we adopt the AMD version of Ref. [15].

In our work, AMD calculations with different EOSs are performed, a soft EOS with the nuclear compressibility $\kappa = 228$ MeV and a stiff EOS with $\kappa = 380$ MeV. The nuclear compressibility is the second derivative of the energy with respect to the density, expressed as

$$\kappa = 9\rho^2 \frac{\partial^2}{\partial \rho^2} \left(\frac{E}{A} \right). \quad (2)$$

Even though recent works set a limitation of the κ value, such as $\kappa = 240 \pm 40$ MeV [18], we use $\kappa = 380$ MeV as an extreme case to study the sensitivity of nuclear stopping to the κ value.

In the study below, in order to explore the sensitivity of the in-medium NN cross section on the nuclear stopping, different NN cross sections are also used, the free NN cross sections, the Li–Machleidt (LM) cross sections [19], which are used in the standard AMD calculation, and the modified version of the LM ones with a free multiplication factor.

In the actual simulations, the calculation of AMD is performed up to 300 fm/c and fragments are formed using a coalescence technique in phase space. The excited fragments further cool down to the ground state, using an afterburner, GEMINI [20], in order to make direct comparisons with the experimental values.

In the following analysis, the same conditions as the INDRA experiment (experimental filters) are applied in the

*zhaominghui@impcas.ac.cn

†huangmeirong@impcas.ac.cn

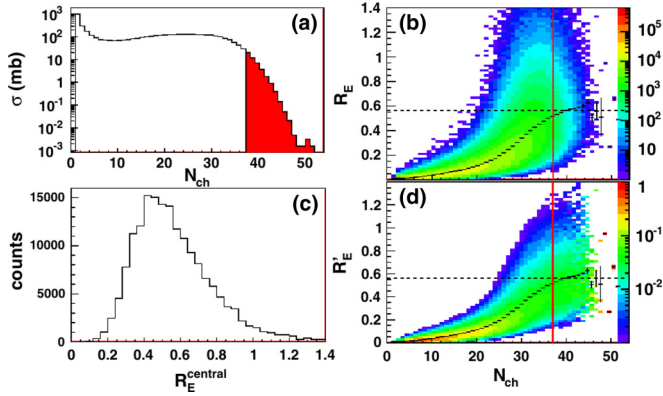


FIG. 1. (Color online) Experimental data for the $^{129}\text{Xe} + ^{120}\text{Sn}$ collisions at 50A MeV. (a) Distribution of total charged-particle multiplicity N_{ch} . The filled area corresponds to the central events used for the analysis of nuclear stopping. (b) Bidimensional plot of the isotropy ratio R_E vs N_{ch} . (c) Distribution of R_E for the central collisions. (d) Same as panel (b), but after renormalizing the number of events in each multiplicity bin of N_{ch} , see Ref. [2].

simulations, which consist of the detectors' angles and energy thresholds. The parameters of these conditions are taken from Ref. [21]. The completeness of the quasiprojectile charged products emitted in the forward velocity space in the center of mass of the reaction is required for the experimentally filtered events; that is, events are taken if the total detected charge Z_{tot} in the forward hemisphere in the center of mass is larger than 80% of the projectile charge. Furthermore, to select the central collision events as done in Ref. [2], the top 50 mb of the high charged-particle multiplicity events are selected for the simulations.

Results. Now we compare our results with the INDRA experimental data of $^{129}\text{Xe} + ^{120}\text{Sn}$ system.

In Figs. 1 and 2, comparisons between experimental data and the simulated results are made under the same conditions to get the value of R_E^{central} [Eq. (1)] of the central collisions. As one can see in Figs. 1 and 2, the overall trend and the distribution of the experimental data are well reproduced by the simulated results. However there are some discrepancies. For the multiplicity distributions, the experimental

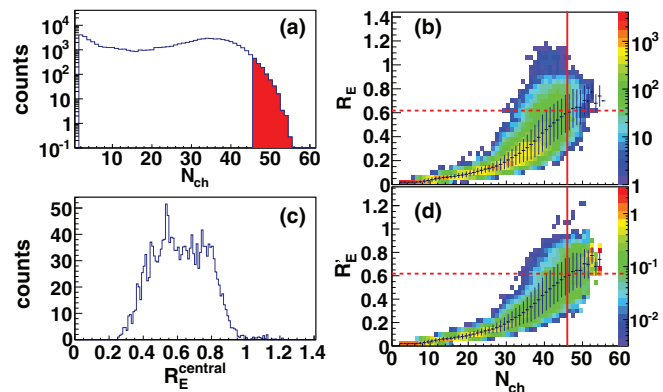


FIG. 2. (Color online) Same plots as Fig. 1, but for the AMD with hard-EOS calculation.

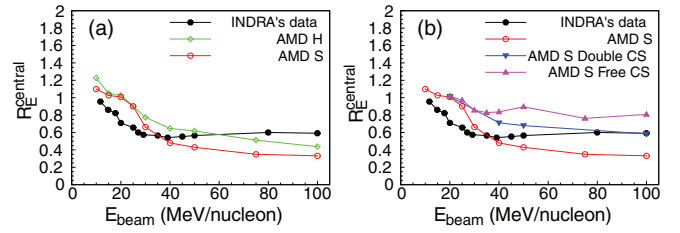


FIG. 3. (Color online) Comparisons between experimental nuclear-stopping values [2] and the predictions of AMD calculations for the central $^{129}\text{Xe} + ^{120}\text{Sn}$ collisions. In panel (a), the black filled circles are the INDRA values, while the red circles and green diamonds are from the AMD calculations of hard and soft EOSs, respectively. In panel (b), black filled circles and red circles are the same as in panel (a), while the purple up triangles are the results of AMD calculations of soft EOSs with free NN cross sections, and the down triangles are those with the Li-Machleidt cross section multiplied by a factor of two.

charged-particle multiplicity in Fig. 1(a) is smaller than that of the simulation in Fig. 2(a) by about 10 units. The experimental R_E distribution in Figs. 1(b) and 1(d) is slightly wider than that of the simulations in Figs. 2(b) and 2(d).

In Fig. 3 the mean value of R_E versus beam energy is plotted for the experimental data of Ref. [2] and those of the simulations. In Fig. 3(a) the simulated results of soft and stiff EOSs are compared with the experimental values. Nuclear stopping becomes larger for the stiff EOS at $E > 30A$ MeV because the stiff-EOS nuclear matter needs more energy to compress than does the soft-EOS nuclear matter. This is consistent with the results of Refs. [11,22]. In Fig. 3(b) the simulated results with the soft EOS, but with different NN cross sections, are compared. For the free NN cross sections, the nuclear stopping becomes roughly independent of the incident energy and shows around 1, the value of complete stopping. For the LM cross sections, the calculated nuclear stopping values are significantly underestimated at $E > 50A$ MeV. When the LM cross sections are multiplied by a factor of two, the stopping values become consistent with those of the INDRA experiment at $E = 75$ and $100A$ MeV. These comparisons indicate that the nuclear-stopping power is sensitive both to EOSs, shown in Fig. 3(a), and to the NN cross sections, shown in Fig. 3(b). Overall, nuclear stopping for different EOSs in Fig. 3(a) shows the same trend as those of the experiments; that is, the stopping power drops as the incident energy increases, then it stays almost constant. Below the Fermi energy, the mean field with Pauli blocking governs the reaction mechanism, while two-body collisions play the decisive role in the reaction at higher energy. Around the Fermi energy, nuclear stopping achieves a minimum in the experimental data, where a mixed effect of the mean field and the NN collisions governs the nuclear reaction mechanism. However, the experimental nuclear stopping below the Fermi energy is not reproduced by any choices of the κ value and the NN cross sections used.

The disagreements of the stopping power R_E between the experimental results and the simulated results at lower energy and at higher energy originate from different reasons. In the

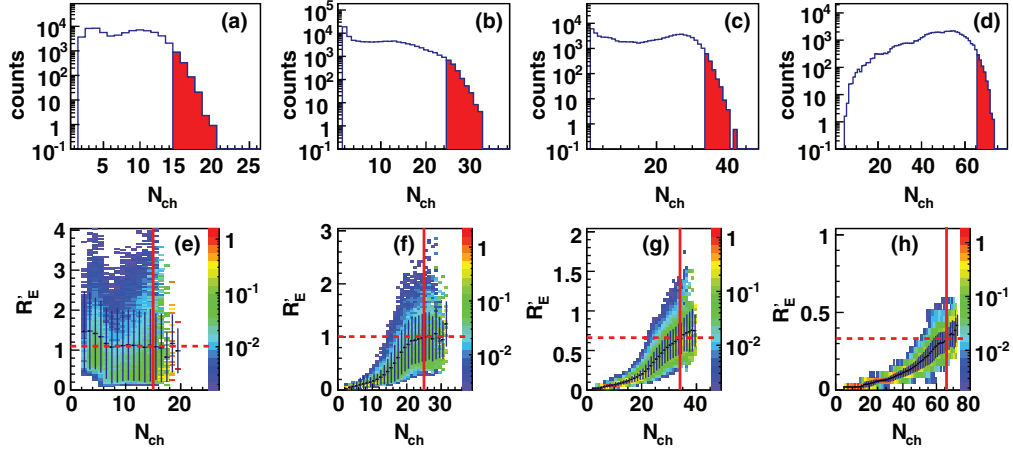


FIG. 4. (Color online) The top four figures are N_{ch} distributions of AMD calculations with the soft EOS and the Li–Machleidt cross sections. The red fill areas correspond to the central collision events. From left to right, the incident energies are 10A MeV, 20A MeV, 30A MeV, 100A MeV. The bottom row corresponds to R_E vs N_{ch} after renormalizing the number of events in each multiplicity bin.

lower-energy region, say below 25A MeV, the calculated nuclear stopping predicts complete nuclear stopping and therefore the stopping does not depend on the stiffness of the EOS and the NN cross sections, whereas the experimental values do not reach complete stopping until the incident energy goes down to $E = 10$ A MeV. The experimental result shows that nuclear stopping decreases from 20A MeV to 40A MeV, then shows a broad minimum at 30 to 40A MeV, a little raising from 40A MeV to 50A MeV, and stays almost constant from 50A MeV to 100A MeV [2]. In the AMD calculations, from 20A MeV to 50A MeV, nuclear stopping decreases more rapidly than those of the experiments for the soft EOS, and the values of nuclear stopping stay nearly constant from 50A MeV to 100A MeV. Here we do not see a minimum of nuclear stopping. For the stiff EOS, the decreases from 20A MeV to 50A MeV becomes similar to that of the experiment. These results at the AMD calculations may be explained as follows. Because increasing the incident energy nuclear stopping caused by the mean field becomes weakened, and at the same time the number of Pauli-allowed collisions is small, so that total nuclear stopping decreases sharply between 20 to 40A MeV. In the energy region above the Fermi energy, the NN collisions become significant because of the weakened Pauli blocking. Therefore, nuclear stopping is largely governed by the in-medium NN cross section, as seen in Fig. 3(b).

Here we would like to mention the effect of the centrality selection of the events. As pointed out before, the AMD simulation predicts a larger multiplicity value than that of the experiment at 50A MeV. As seen in Figs. 1(b), 1(d) and Figs. 2(b), 2(d), the mean value of R_E increases with increasing multiplicity. Therefore the lower charged-particle multiplicity value in the experimental data may results in lower nuclear stopping or vice versa. In order to study the effect of the disagreement of the charged-particle multiplicity on nuclear stopping, the relation between nuclear stopping and charged-particle multiplicity is studied.

In Fig. 4 the selection of the central events at 10, 20, 30, and 100A MeV and the corresponding figures of R_E vs the charged-particle multiplicity N_{ch} are shown. As one can see,

at 10A MeV the AMD-calculated result of nuclear stopping vs N_{ch} is very different from that of the higher energies. Nuclear stopping stays more or less independent of the N_{ch} values, indicating that the N_{ch} value is mainly determined by the fluctuation of the detected-particle multiplicity, but not by the centrality of the reaction. In the higher-energy reactions, on the other hand, the correlation between the R_E and N_{ch} becomes more linear and the R_E distribution at a given N_{ch} becomes narrower as N_{ch} increases. At energies of 20 and 30A MeV, the linear increase of nuclear stopping stops at a certain N_{ch} value and the stopping starts to saturate. Even at 100A MeV, the maximum value of nuclear stopping is almost obtained at the N_{ch} values corresponding to 50 mb of the central collision selection. Therefore these studies indicate that the different N_{ch} values in the experiment and the simulations cause only minor effects on nuclear stopping and do not explain the discrepancy between the experiment and the simulations seen in Fig. 3.

Summary and conclusions. From the AMD calculations, we found that nuclear stopping is sensitive to both the EOS and the in-medium NN cross section, and therefore nuclear stopping can be a good probe to study both of them. Both AMD calculations and the experiment of INDRA show that nuclear stopping becomes maximum at the lowest-energy region, $E = 10$ A MeV in the experiment and $E < 25$ A MeV in the simulations, and starts to decrease as the incident energy increases up to 40A MeV (Fermi energy). In the 20 to 40A MeV, the energy dissipation derived from mean field remains dominant and the NN collision contribution remains small, resulting in the decreasing trend of nuclear stopping. Above 50A MeV, the NN collisions govern nuclear stopping and provide the nuclear stopping measurement as a good probe to study the in-medium NN collision cross section.

However, significant discrepancies in nuclear stopping between the experiments and the AMD simulations are observed below the Fermi energy region, which makes it difficult to set limitation on the κ value and the in-medium NN cross section in this study. This discrepancy originates

neither from the stiffness of the EOS nor the values of the in-medium NN cross section. The difference in the centrality selection of the events seems not to be the cause neither. The experimental results somehow show much larger transparency of the nucleons at this energy range. Further investigations are needed to solve this discrepancy.

Acknowledgments. We would like to acknowledge the HIRFL supercomputing center. This work is financially supported by the National Basic Research Program of China

(973 Program) with Grant No. 2014CB845405 and by the National Natural Science Foundation of China with Grants No. 11205209, No. 11205221, No. 11075190, No. 11005127, No. 11105187, and No. 11075189, by the 100 Persons Project (Grants No. 0910020BR0 and No. Y010110BR0), and by the ADS project 302 (Grant No. Y103010ADS) of the Chinese Academy of Sciences. One of the author (R. Wada) thanks the Chinese Academy of Science for their support for visiting senior international scientists.

-
- [1] J. Lattimer and M. Prakash, *Astrophys. J.* **550**, 426 (2001).
[2] G. Lehaut, D. Durand *et al.* (INDRA and ALADIN Collaborations), *Phys. Rev. Lett.* **104**, 232701 (2010).
[3] A. Carbone, G. Colò *et al.*, *Phys. Rev. C* **81**, 041301 (2010).
[4] K. S. Vinayak and S. Kumar, *J. Phys. G* **39**, 095105 (2012).
[5] J.-Y. Liu, W.-J. Guo *et al.*, *Phys. Rev. Lett.* **86**, 975 (2001).
[6] W. Scheid, H. Müller, and W. Greiner, *Phys. Rev. Lett.* **32**, 741 (1974).
[7] H. A. Gustafsson, H. H. Gutbrod *et al.*, *Phys. Rev. Lett.* **52**, 1590 (1984).
[8] J. J. Molitoris and H. Stöcker, *Phys. Lett. B* **162**, 47 (1985).
[9] A. Ono, H. Horiuchi, T. Maruyama, and A. Ohnishi, *Prog. Theor. Phys.* **87**, 1185 (1992).
[10] A. Ono and H. Horiuchi, *Prog. Part. Nucl. Phys.* **53**, 501 (2004).
[11] R. Wada, T. Keutgen *et al.* (NIMROD Collaboration), *Phys. Rev. C* **69**, 044610 (2004).
[12] A. Ono, H. Horiuchi, T. Maruyama, and A. Ohnishi, *Phys. Rev. Lett.* **68**, 2898 (1992).
[13] T. Maruyama, K. Niita, and A. Iwamoto, *Phys. Rev. C* **53**, 297 (1996).
[14] Y. Kanada-En'yo, H. Horiuchi, and A. Doté, *J. Phys. G* **24**, 1499 (1998).
[15] A. Ono, *Phys. Rev. C* **59**, 853 (1999).
[16] Y. Kanada-En'yo, M. Kimura, and H. Horiuchi, *C. R. Phys.* **4**, 497 (2003).
[17] Y. Kanada-En'yo, M. Kimura, and A. Ono, *Prog. Theor. Exp. Phys.* (2012) 01A202.
[18] G. Colò, N. Van Giai, J. Meyer, K. Bennaceur, and P. Bonche, *Phys. Rev. C* **70**, 024307 (2004).
[19] G.-Q. Li and R. Machleidt, *Phys. Rev. C* **49**, 566 (1994).
[20] R. Charity, M. McMahan *et al.*, *Nucl. Phys. A* **483**, 371 (1988).
[21] J. Pouthas, B. Borderie *et al.*, *Nucl. Instrum. Methods Phys. Res., Sect. A* **357**, 418 (1995).
[22] G. Q. Zhang, Y. G. Ma *et al.*, *Phys. Rev. C* **84**, 034612 (2011).